Efficient Digital Control for MPP Tracking and Output Voltage Regulation of Partially Shaded PV Modules in DC Bus and DC Microgrid Systems

Moustafa Adly, *Student Member, IEEE*, and Kai Strunz

***Abstract*—The integration of photovoltaic (PV) modules into dc microgrids relies on the capabilities of maximum power point (MPP) tracking and output voltage regulation (OVR). Under partial shading or mismatches between PV submodules, accurate global MPP tracking and efficient OVR are challenging processes. For global MPP tracking, the distributed MPP tracking is a potential solution but comes at the expense of increased system complexity. For the OVR, operating the PV module in its current source region would result in rather high power losses in the converter circuit and, thus, in increased heat accumulation. The existence of multiple current source regions in the mismatched PV characteristics complicates the control design. The novel digital controller for module integrated converters developed here supports the effective integration of mismatched and partially shaded PV modules while employing a minimal number of sensors. The proposed double-stage global MPP tracking algorithm realizes fast and accurate MPP tracking with neither periodic scanning nor oscillations around the optimum. For the OVR, the algorithm targets the reduction of the converter power losses through effective allocation of the PV operating point. A prototype of the control is realized as a proof of concept.**

***Index Terms*—DC microgrid, global maximum power point (MPP) tracking, module integrated converter (MIC), output voltage regulation (OVR), partial shading, photovoltaics (PVs).**

I. Introduction

DC microgrids have recently spread to numerous applications [1], [2]. A variety of current structures are available for integrating photovoltaics (PVs) in such dc microgrids [2]–[4]. Centralized, multi-string, string, module, and submodule integration levels represent the main PV integration topologies [3], [5], [6]. Module-level integration via so-called module integrated converters (MICs) is characterized by high power efficiency, decentralized control, fault tolerance, and flexible integration [6], [7]. These MICs are particularly suitable for residential and low-voltage applications where size and cost are important decision factors [7], [8].

Manuscript received August 7, 2018; accepted September 27, 2018. Date of publication October 14, 2018; date of current version May 2, 2019. Recommended for publication by Associate Editor V. Agarwal. This work was supported in part by DAAD and in part by the project OptNetzE (0325814A) funded by the Federal Ministry for Economic Affairs and Energy (BMWi).
(Corresponding author: Moustafa Adly.)

The authors are with the Sustainable Electric Networks and Sources of Energy, Technische Universität Berlin, Berlin D-10587, Germany (e-mail: m.adly@mailbox.tu-berlin.de; kai.strunz@tu-berlin.de).

Color versions of one or more of the figures in this paper are available online at http://ieeexplore.ieee.org.

Digital Object Identifier 10.1109/TPEL.2018.2873753

Maximum power point (MPP) tracking and output voltage regulation (OVR) represent the two control modes of a MIC [9]. Both control modes are influenced by the existence of multiple local maxima and one global MPP on the power–voltage characteristics of the PV module [10]–[13]. The existence of several local maxima is attributed to the mismatch between the submodules due to fabrication tolerances, dust accumulation, or partial shading [10]–[12], [14]. In this context, the efficacy of both control modes relies on various factors. For the global MPP tracking mode, on the one hand, the utilized number of sensors, speed and accuracy of tracking, ease of implementation, and cost are used for quality assessment [15]–[19]. On the other hand, tight dc bus voltage control and balanced power sharing between sources, as well as low converter power losses and the corresponding reduced heat accumulation, are the indicators of the quality of the OVR mode [9], [20]–[27].

In this paper, a novel digital controller for integrating PV modules into dc microgrid systems is developed. Compared with the existing controllers [5], [7], [11], [12], [19], it is distinguished in that the proposed controller is of a leaner structure with fewer sensors. In [7], the number of sensors is greater than double the number of submodules. However, for image processing of the partial shading pattern, four sensors are utilized in [19]. At least two sensors are used in [11], [13], and [14]. In this paper, only one sensor is utilized for global MPP tracking. This results in less measurement power loss and reduced size and cost. For the MPP tracking mode, fast and accurate tracking is attained by the precise determination of the perturbation and sampling times. So far, these times have been considered in three main ways in the scientific literature. At first, they were obtained from experimental and simulation results [7], [14]. Second, arbitrary values employing sufficient safety margins were utilized [11], [13]. Third, the number of tracking samples was used for analyzing the speed of the MPP algorithm [18]. In this paper, a closed form of the sampling time that takes the parasitics of the converter elements into account is provided. This facilitates obtaining a realistic estimation of the perturbation time. Furthermore, the oscillations around the global MPP resulting from the tracking algorithm or limit cycle oscillations are suppressed. This is important. Oscillation around the global MPP is a common issue in most MPP tracking techniques [15], [19], [28]. Such oscillations have shown to be the cause of power quality problems [29].

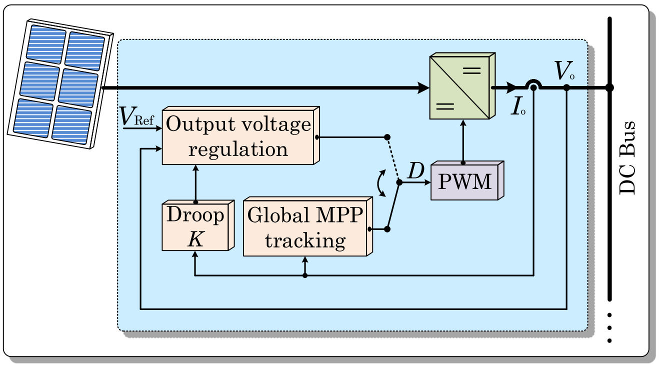

Fig. 1. Structure of the proposed PV module integration into dc microgrids.

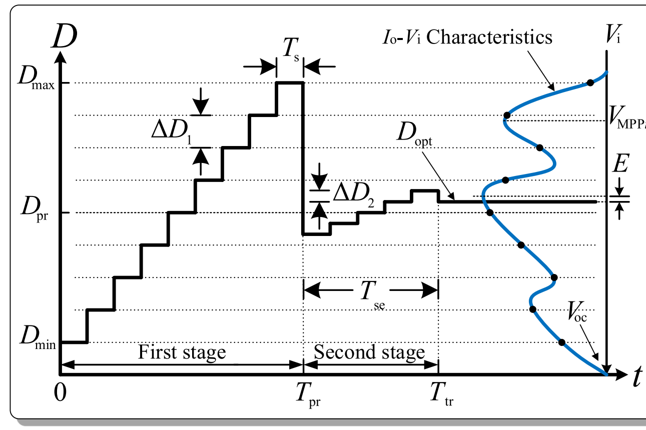

Fig. 2. Parameters and performance of the double-stage global MPP tracking algorithm.

The power losses in the converter circuit result in heat accumulation. The latter adversely influences the lifetime of the converter elements [27]. Therefore, for less power losses of the converter in the OVR mode, the PV module is operated in its voltage source region [21], [22]. Under mismatch conditions, multiple voltage source regions exist. Locating the PV operating point in the highest appropriate PV voltage source region is a challenge addressed in this paper.

Following this introduction, the novel global MPP tracking technique is presented in Section II. In Section III, the OVR mode and its design are illustrated. The standalone and dc bus system applications are discussed in Section IV. The test system and parameter design for both control algorithms are introduced in Section V. Experimental validation and prototyping are discussed in Section VI. Finally, conclusions are drawn in Section VII. In the Appendix, the simulation results of mode transition between global MPP tracking and OVR are presented.

II. Global MPP Tracking

In this section, the novel global MPP tracking mode is developed. As a part of the PV system control, the global MPP tracking controller is shown in Fig. 1. The influence of the developed algorithm on the system structure and required sensing elements are discussed in Section II-A. Then, the concept and parameters of the proposed global MPP tracking algorithm are introduced in Section II-B. In Section II-C, the conditions for resetting the global MPP tracking algorithm and mode transition are developed. The tracking accuracy is evaluated in Section II-D.

A. Sensing Elements for Global MPP Tracking

In state-of-the-art tracking techniques, the solar irradiance and converter input voltage and current are commonly measured for global MPP tracking of partially shaded PV modules [10]–[12]. Therefore, sensors for irradiance, voltage, and current are employed. The number of sensors impacts the measurement losses, size and complexity, and cost of the MIC. In the case of dc bus and microgrid systems where the dc voltage is tightly regulated, however, the number of sensors may be reduced. This is because the maximization of the converter output current, then, effectively results in harvesting the maximum PV power. Thus, a converter output current sensor is sufficient for global MPP tracking. Furthermore, this one sensor is already to be installed for the purpose of droop control in the OVR mode too, but sensors for irradiance and converter input voltage and current are omitted. As a result, the measurement losses are reduced.

B. Double-Stage Global MPP Tracking

For global MPP tracking, the characteristic of the converter output current I_o versus the PV voltage V_i is important. This characteristic is representative of the PV power P_i versus the PV voltage V_i characteristic, assuming a constant dc bus voltage V_o, and it is utilized for MPP tracking. Thus, irrespective of the PV voltage V_i, maximizing the converter output current I_o results in harvesting the maximum PV power since V_o is approximated as a constant. This assumption is justified in the dc microgrid. Therefore, only the converter output current I_o is measured, while the need to measure the PV voltage V_i is omitted.

The global MPP tracking algorithm consists of two stages, as shown in Fig. 2, where tracking times T_{pr} and T_{se} refer to the primary and secondary stages, respectively. In the first stage, the I_o–V_i characteristic is scanned. The pulsewidth modulation (PWM) duty ratio D is varied from a minimum $D_{\min}$ to a maximum $D_{\max}$ in steps of ΔD_1 while recording the corresponding converter output currents. After each step, the duty ratio is maintained for an interval T_s to allow for the output current to settle. As a result of the first stage, the primary duty ratio D_{pr} corresponding to the maximum output current is known. Then, a second global MPP tracking stage is activated.

The second stage serves to improve the tracking accuracy. The vicinity of the obtained D_{pr} is scanned in duty ratio steps ΔD_2 that are smaller than ΔD_1. The scanning window in this case is $[D_{pr} - \Delta D_1 + \Delta D_2, D_{pr} + \Delta D_1 - \Delta D_2]$. The optimal duty ratio D_{opt} corresponding to the global maximum output current is so determined. This marks the end of the tracking process, and the PWM is further activated with D_{opt}.

The total tracking time T_{tr}, the optimal duty ratio D_{opt}, and the tracking error E are shown in Fig. 2. Thus, the parameters of the global MPP tracking algorithm are T_s, $D_{\min}$, $D_{\max}$, ΔD_1, and ΔD_2. These are determined as follows.

1) Settling Time T_s: Following a step change of the duty ratio in the scanning process, the converter output current I_o changes and settles within the time interval T_s. For accurate global MPP tracking, the current I_o is to be measured after settling. Therefore, employing rather small values for T_s may compromise the tracking accuracy. In contrast, the use of relatively large safety margins in setting T_s increases the total tracking time T_{tr}. This observation motivates an accurate determination of T_s. For this purpose, the small-signal transfer function $i_o(s)/d(s)$ relating the output current to the duty ratio is utilized. For the small-signal modeling of the boost converter [30], the continuous conduction mode is assumed, as can be ensured through the choice of the converter inductance L and the switching frequency f_{sw} depending on the irradiance [6]. The small-signal transfer function is given by [30]

$$\frac{i_o(s)}{d(s)} = A \cdot \frac{(C_o \cdot r_{C_o} \cdot s + 1)\left(s - \frac{\frac{V_o}{I_o}\cdot(1-D)^2 - r_{SL}}{L}\right)}{s^2 + 2\cdot\zeta\cdot\omega_n\cdot s + \omega_n^2} \quad (1)$$

with

$$A = \frac{-I_o}{(1-D)\cdot C_o \cdot \left(\frac{V_o}{I_o} + r_{C_o}\right)}$$

$$\zeta\cdot\omega_n = \frac{C_o\cdot\left[r_{SL}\cdot\left(\frac{V_o}{I_o}+r_{C_o}\right) + (1-D)^2\cdot\frac{V_o}{I_o}\cdot r_{C_o}\right] + L}{2\cdot L\cdot C_o\cdot\left(\frac{V_o}{I_o}+r_{C_o}\right)}$$

$$\omega_n^2 = \frac{r_{SL} + (1-D)^2\cdot\frac{V_o}{I_o}}{L\cdot C_o\cdot\left(\frac{V_o}{I_o}+r_{C_o}\right)}$$

where D is the steady-state duty ratio, r_{SL} is the equivalent parasitic resistance of the inductor and switching elements, C_o is the output capacitance, r_{C_o} is the equivalent series resistance of the output capacitor, V_o is the steady-state output voltage, and I_o is the steady-state output current. The settling time $T_s = 4/(\zeta\cdot\omega_n)$ [31] is, thus, given by

$$T_s = \frac{8\cdot L\cdot C_o\cdot\left(\frac{V_o}{I_o}+r_{C_o}\right)}{C_o\cdot\left[r\cdot\left(\frac{V_o}{I_o}+r_{C_o}\right) + (1-D)^2\cdot\frac{V_o}{I_o}\cdot r_{C_o}\right] + L}. \quad (2)$$

Accounting for the various values of D and I_o and the components' tolerances, the maximum T_s from (2) is retained.

2) Minimum Duty Ratio D_{min}: The duty ratio D of the boost converter with input voltage V_i and dc bus voltage V_o is given by

$$D = 1 - \frac{V_i}{V_o}. \quad (3)$$

Since the dc bus voltage is nearly constant, the minimum duty ratio corresponds, then, to the maximum input voltage. For a minimal scanning window and, thus, less tracking time, the maximum input voltage is set equal to the voltage of the one power peak that has the highest PV module output voltage. The latter is determined as follows. For a PV module composed of n submodules with an open-circuit voltage V_{oc}/n for each submodule, the maximum possible number of power peaks on the module power–voltage characteristic is equal to n [10]. Furthermore, the voltage V_{MPPi} of the power peak number i [15] is approximated as follows:

$$V_{MPPi} = \frac{0.8\cdot i\cdot V_{oc}}{n}, \qquad 1 \leqslant i \leqslant n. \quad (4)$$

However, in [13], [28] and [32], a small voltage shift of V_{MPPi} for the power peaks given by (4) was determined. Therefore, in order not to skip the power peak of voltage V_{MPPn}, the maximum input voltage employed in (3) for determining D_{min} is considered as $V_i = V_{oc}$. Furthermore, the maximum V_{oc} corresponding to the minimum operating temperature is employed. Thus, for analog control, $D_{min,analog}$ is given by

$$D_{min,\,analog} = 1 - \frac{V_{oc}}{V_{omin}} \quad (5)$$

where V_{omin} is the minimum value of the dc bus voltage. However, for digital control, the value of D_{min} is chosen as an integer multiple of the minimum duty ratio step ΔD_{min} of the employed digital control chip to avoid limit cycle oscillation. For this purpose, the floor function is utilized to obtain the minimum duty ratio employed in the digital control chip as follows:

$$D_{min} = \left\lfloor \frac{1 - V_{oc}/V_{omin}}{\Delta D_{min}} \right\rfloor \cdot \Delta D_{min} \quad (6)$$

where $\lfloor x \rfloor$ is the largest integer that is less than or equal to x.

3) Maximum Duty Ratio D_{max}: The maximum duty ratio D_{max} corresponds to the minimum scanned input voltage in (3). The latter represents the voltage V_{MPP1} of the first power peak obtained from (4) as $V_{MPP1} = 0.8\cdot V_{oc}/n$. Thus, substituting the right-hand side of V_{MPP1} into (3) yields

$$D_{max,\,analog} = 1 - \frac{0.8\cdot V_{oc}}{n\cdot V_{omax}} \quad (7)$$

where V_{omax} is the maximum value of the dc bus voltage V_o. For the digital control chip, the maximum duty ratio is determined using the ceil function as follows:

$$D_{max} = \left\lceil \frac{1 - 0.8\cdot V_{oc}/(n\cdot V_{omax})}{\Delta D_{min}} \right\rceil \cdot \Delta D_{min} \quad (8)$$

where $\lceil x \rceil$ is the smallest integer that is greater than or equal to x.

For a PV module comprising three submodules, a representative power versus voltage characteristic under mismatch is shown in Fig. 3. The trajectories of D_{min} and D_{max}, the global MPP scanning domain, and the local and global MPPs are depicted.

4) Secondary Duty Ratio Step ΔD_2: The selection of the duty ratio step ΔD_2 applied in the second tracking stage affects the accuracy of tracking the global MPP. Smaller values result in more accurate tracking. However, too small a value of ΔD_2 may result in a change of I_o that is undetectable by the analog to digital converter (ADC) of the control chip. Therefore, the change of D that results in the minimum detectable change of I_o is to be determined. Thus, the small-signal transfer function $i_o(s)/d(s)$ of (1) is utilized. A step change of magnitude k_i in the duty ratio $d(s) = k_i/s$ results in a change of the converter

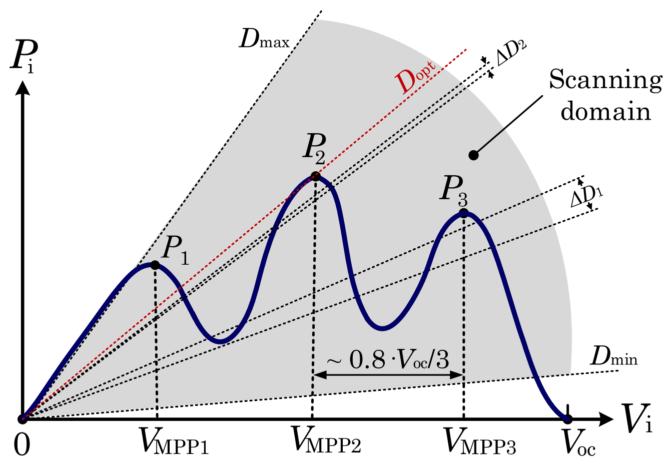

Fig. 3. Power versus voltage characteristics of a mismatched module with the global MPP scanning range.

output current ΔI_o. From the final-value theorem, the steady-state value of ΔI_o is calculated using the small-signal transfer function $i_o(s)/d(s)$ as follows:

$$|\Delta I_o| = \left| \lim_{s\to 0} s \cdot \frac{k_i}{s} \cdot \frac{i_o(s)}{d(s)} \right|. \tag{9}$$

The value of $|\Delta I_o|$ must be greater than the minimum detectable current change ΔI_{omin}. The latter is determined as follows. For an ADC with maximum voltage V_{ADC} and N_{ADC} bits for the analog-to-digital conversion process, ΔI_{omin} is given by

$$\Delta I_{omin} = \frac{V_{ADC}}{G_i \cdot 2^{N_{ADC}}} \tag{10}$$

where G_i is the converter output current sensing gain. The minimum value of the magnitude $k_i = k_{imin}$ is obtained by equating (9) to (10) as follows:

$$k_{imin} = \frac{V_{ADC}}{G_i \cdot 2^{N_{ADC}} \cdot \left| \lim_{s\to 0} \frac{i_o(s)}{d(s)} \right|}. \tag{11}$$

The employed ΔD_2 is, then, set to

$$\Delta D_2 = m_{min} \cdot \Delta D_{min} \tag{12}$$

where $m_{min} = \lceil k_{imin}/\Delta D_{min} \rceil$. Thus, employing an ADC with larger N_{ADC} reduces k_{imin} and, hence, ΔD_2. As a result, the integer m_{min} is reduced for precise global MPP tracking.

5) Primary Duty Ratio Step ΔD_1: The duty ratio step ΔD_1 of the first tracking stage influences the speed and accuracy of tracking the global MPP. Larger values reduce the number of tracking cycles and, thus, the tracking time. However, this may result in skipping the scanning of any of the power peaks. Therefore, two conditions for setting ΔD_1 are derived as follows. Through the first condition, the ΔD_1 that minimizes the tracking time T_{tr} is obtained. The latter is given by

$$T_{tr} = T_{pr} + T_{se} \tag{13}$$

with

$$T_{pr} = \left(\frac{D_{max} - D_{min}}{\Delta D_1} + 1 \right) \cdot T_s$$

$$T_{se} = \left(\frac{2 \cdot \Delta D_1 - 2 \cdot \Delta D_2}{\Delta D_2} + 1 \right) \cdot T_s$$

where T_{pr} and T_{se} are the scanning time intervals of the primary and secondary stages, respectively. For fixed D_{min}, D_{max}, and ΔD_2, the expression of T_{tr} is differentiated with respect to ΔD_1 and equated to zero in order to find the optimal T_{tr}. The minimum tracking time T_{tr} is so obtained for

$$\Delta D_1 = \sqrt{\frac{1}{2} \cdot \Delta D_2 \cdot (D_{max} - D_{min})}. \tag{14}$$

In the second condition, the maximum employed ΔD_1 to avoid skipping the detection of any of the power peaks in the scanning process is determined. For this purpose, the minimum voltage difference between two adjacent peaks on the I_o versus V_i characteristic of the PV module is considered. From (4), the voltage difference between two adjacent peaks V_{MPPi} and $V_{MPP(i+1)}$ is equal to $0.8\, V_{oc}/n$. The variation of D that results in this PV voltage variation represents the upper limit of ΔD_1 and is determined as follows. From (3), the rate of change of the duty ratio with respect to the PV module voltage is obtained from

$$\frac{dD}{dV_i} = \frac{-1}{V_o} \tag{15}$$

assuming negligible variation of the dc bus voltage V_o. According to (3), a $\Delta D > 0$ reduces V_i. Approximating in (15) $\Delta D = dD$ and $\Delta V_i = dV_i$ gives

$$\Delta D = \frac{-\Delta V_i}{V_o}. \tag{16}$$

Replacing $-\Delta V_i$ of (16) by the voltage difference between two adjacent power peaks results in the upper limit ΔD_{1max} of the primary duty ratio step ΔD_1 as follows:

$$\Delta D_{1max} = \frac{0.8 \cdot V_{oc}}{n \cdot V_o}. \tag{17}$$

To satisfy the two mentioned conditions, ΔD_1 is chosen as

$$\Delta D_{1,analog} = \min \left\{ \sqrt{\frac{\Delta D_2 \cdot (D_{max} - D_{min})}{2}}, \frac{0.8 \cdot V_{oc}}{n \cdot V_o} \right\}. \tag{18}$$

The employed ΔD_1 is, then, set to

$$\Delta D_1 = l_{min} \cdot \Delta D_{min} \tag{19}$$

where $l_{min} = \lfloor \Delta D_{1,analog}/\Delta D_{min} \rfloor$.

C. Resetting and Mode Transition

1) Resetting Global MPP Tracking Algorithm: Variations of the irradiance or of the shading pattern influence the converter output power and, accordingly, its output current I_o. Hence, for detecting such variations, I_o is continuously measured upon employing D_{opt}. The magnitude of current difference δI_o between the successive measurements is recorded. Having δI_o

greater than a critical practical limit δI_{ocr} indicates a considerable change of the irradiance or shading pattern. As a result, the global MPP tracking algorithm is reset, and a new tracking process takes place. In this manner, the need for periodic scanning of the PV power versus voltage characteristics is overcome.

2) Mode Transition to OVR: Upon determining D_{opt} through the second global MPP tracking stage, the converter output voltage V_{o} is sensed continuously. A transition to the OVR mode is to take place when the sensed V_{o} exceeds its upper boundary. This upper boundary is $V_{\mathrm{ref}} + \Delta V_{\mathrm{o}}$, where V_{ref} and ΔV_{o} are the nominal dc bus voltage and its maximum allowed deviation considering droop effects, respectively. A violation of this boundary is an indicator of having a higher power generation than consumption over a certain time interval. Thus, the PV power is reduced by switching to the OVR mode.

D. Tracking Accuracy

The tracking error E depicted in Fig. 2 is a measure of the tracking accuracy. This error represents the voltage difference between the true PV voltage V_{GMPP} giving maximum power and the actually tracked PV voltage. This error is at its maximum when the voltage of the global MPP lies in the middle of two voltage levels separated by a duty ratio perturbation of ΔD_2. Therefore, the maximum absolute value of E is given by

$$E_{\max} = \frac{|\Delta V|}{2} \tag{20}$$

where ΔV is the PV module voltage variation corresponding to a duty ratio change of ΔD_2. Inserting (16) into (20) with $\Delta V_{\mathrm{i}} = \Delta V$ and $\Delta D = \Delta D_2$, $E_{\max}$ is given by

$$E_{\max} = \frac{|\Delta D_2| \cdot V_{\mathrm{o}}}{2}. \tag{21}$$

With the insertion of (12), we obtain

$$E_{\max} = \frac{m_{\min} \cdot \Delta D_{\min} \cdot V_{\mathrm{o}}}{2}. \tag{22}$$

For a digital control chip with N_{PWM} bits for the PWM module, $\Delta D_{\min}$ is equal to $1/2^{N_{\mathrm{PWM}}}$. Thus, the absolute maximum tracking error is given by

$$E_{\max} = \frac{m_{\min} \cdot V_{\mathrm{o}}}{2^{N_{\mathrm{PWM}}+1}}. \tag{23}$$

From Section II-B4, $E_{\max}$ is reduced by employing an ADC with a larger N_{ADC}.

III. Output Voltage Regulation

As an alternate PV integration control mode, the OVR and the novel developed algorithm are presented in the following. In addition, the mode transition conditions are investigated.

A. OVR Algorithm

The load power in dc bus and dc microgrid systems is determined from the bus voltage and the total equivalent load resistance. At a given load resistance, supplying the dc bus at the level of the consumed load power keeps the dc bus voltage unchanged. Thus, at a given load power, power generation higher than consumption results in an increasing dc bus voltage and vice versa. For such power balancing, therefore, specific amounts of the PV power are to be provided by the MIC.

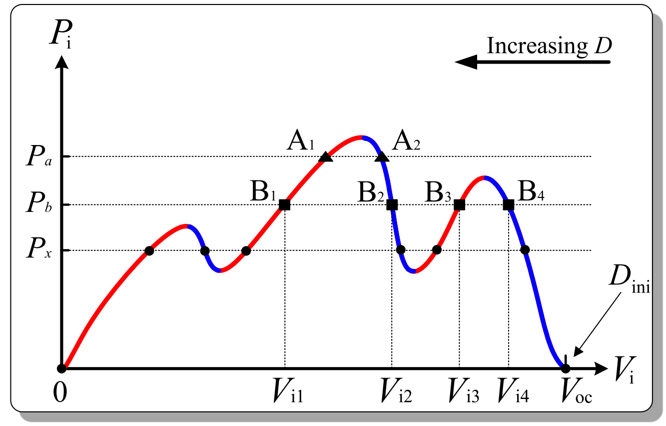

Fig. 4. Current source (red) and voltage source (blue) regions of partially shaded PV module and different operating points at different PV power levels.

Under uniform irradiance, the characteristic of the PV power P_{i} versus the PV voltage V_{i} always gives two operating points that deliver the same PV power. These P_{i} versus V_{i} characteristics and their corresponding PV current versus PV voltage characteristics are divided into current source, maximum power, and voltage source regions [21], [22]. Thus, for a specific PV power, one of the two PV operating points is in the current source region, and the other one is in the voltage source region. Relative to operation in the voltage source region, the operation in the current source region results in a larger PV current and a higher power loss in the converter [6]. This higher power loss reduces the lifetime of the converter elements [27].

Under partial shading, multiple voltage and current source regions exist, as shown in Fig. 4. For a lower PV current and lower power losses in the converter circuit, points B_1, B_2, and B_3 in the figure are undesirable; point B_4 is preferred instead. Thus, in Fig. 4, a certain PV power P_b is obtained by operating the PV module at a voltage V_{i1}, V_{i2}, V_{i3}, or V_{i4}. Although point B_2 represents operation in a voltage source region, point B_4 is yet better due to its lower current. Thus, in general, for a set of m PV voltages $\{V_{\mathrm{i1}}, V_{\mathrm{i2}}, \ldots, V_{\mathrm{i}m}\}$ that produce the same PV power P_x, it is aimed to operate the PV module at the voltage V_{i} such that

$$V_{\mathrm{i}} = \max\{V_{\mathrm{i1}}, V_{\mathrm{i2}}, \ldots, V_{\mathrm{i}m}\} : \\ P_{\mathrm{i}}(V_{\mathrm{i}j}) = P_x \quad \forall \quad j \in \{1, 2, \ldots, m\} \tag{24}$$

where P_x represents the PV power to maintain the power balance sufficient for keeping the dc bus voltage V_{o} unchanged.

Following the approach taken for the global MPP tracking algorithm, a scanning process is also adopted in the OVR algorithm. The P_{i} versus V_{i} characteristic is scanned by varying the PWM duty ratio. In the following, the scanning process and the block diagram representation of the control shown in Fig. 5 are presented.

The scanning process starts at a minimum duty ratio D_{ini} that corresponds to the module open-circuit voltage V_{oc}, as shown

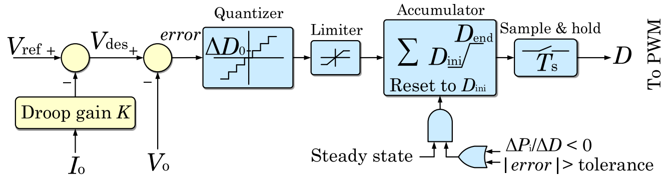

Fig. 5. Block diagram of the developed OVR control algorithm.

in Fig. 4. This value represents the initial condition of the accumulator shown in Fig. 5.

The value of $D_{\rm ini}$ is employed in the PWM for a time interval $T_{\rm s}$ to allow for the converter output voltage settling. The resulting converter output voltage $V_{\rm o}$ is compared with $V_{\rm des}$ to determine the bus voltage error. For uniform power sharing, droop control is employed for determining $V_{\rm des}$, as shown in Fig. 5. This error is, then, scaled and quantized in steps of $\Delta D_{\rm o}$. Having rather large quantizer outputs may speed up reaching the desired bus voltage. However, this may result in moving the PV operating point to a current source region when a local power peak is approached. Therefore, the quantizer output is fed to a limiter to put a bound on the magnitude of the duty ratio change. The limiter output is, then, accumulated and employed in the PWM for an interval $T_{\rm s}$. The scanning process is maintained by repeating the loop until $V_{\rm o}$ reaches the desired level or D exceeds its maximum $D_{\rm end}$. The value of $D_{\rm end}$ represents the end of the scanning window and is chosen to avoid damaging the converter switches.

At the steady state, the accumulator is reset to $D_{\rm ini}$ in two cases. The first case is activated when the bus voltage error exceeds its allowed tolerance. The second case applies when operation in a current source region is detected upon settling. For detection of the latter case, the slope $\Delta P_{\rm i}/\Delta V_{\rm i}$ is examined by the controller. Since $\Delta V_{\rm i}$ and ΔD are related by (16), the PV operating point is in the current source region if $\Delta P_{\rm i}/\Delta D < 0$. The developed OVR algorithm parameters are $T_{\rm s}$, $D_{\rm ini}$, and $\Delta D_{\rm o}$. They are determined in the following.

1) Settling Time $T_{\rm s}$: For the OVR algorithm, $T_{\rm s}$ represents the settling time of the converter output voltage following a step change of the duty ratio. In dc applications with pure resistive loads, the converter output voltage and current have almost similar dynamics [17], [30]. Therefore, $T_{\rm s}$ obtained from (2) is sufficient for the converter output voltage settling and is, therefore, utilized in the OVR algorithm.

2) Initial Duty Ratio $D_{\rm ini}$: It represents the starting point of the scanning window. This is obtained by inserting the maximum PV voltage and the minimum dc bus voltage in (3). The open-circuit voltage $V_{\rm oc}$ represents the maximum PV input voltage. The minimum dc bus voltage is estimated from the allowed deviations of the bus voltage. In dc microgrids, tolerances of up to 10 % in the dc bus voltage are given [9]. For the worst-case analysis while starting the OVR, it has been assumed that the dc bus voltage is around 80 % of its rated values. Therefore, and due to the unregulated bus voltage during the transition to the OVR mode, it was found that $D_{\rm ini}$ can be computed using

$$D_{\rm ini} \leqslant 1 - 1.25 \cdot \frac{V_{\rm oc}}{V_{\rm omin}}. \tag{25}$$

The scaling factor of 1.25 represents a safety margin in order that the scanning starts from an output voltage below $V_{\rm oc}$. The value of $D_{\rm ini}$ has to be an integer multiple of $\Delta D_{\rm min}$ to avoid limit cycle oscillation.

3) OVR Duty Ratio Step $\Delta D_{\rm o}$: The minimum duty ratio step $\Delta D_{\rm o}$ is the duty ratio step that results in the minimum converter output voltage change detectable by the ADC. For computing its value, the converter output voltage to duty ratio small-signal transfer function $v_{\rm o}(s)/d(s)$ is utilized. A procedure similar to the one used for determining ΔD_2 in Section II-B4 using (9) and (10) is followed. Thus, similarly, for an output voltage sensing gain $G_{\rm v}$, the magnitude $k_{\rm v}$ of the duty ratio step change representing the minimum $\Delta D_{\rm o}$ is determined from

$$k_{\rm v}^{-1} = \left| \lim_{s \to 0} \frac{v_{\rm o}(s)}{d(s)} \right| \cdot \frac{G_{\rm v} \cdot 2^{N_{\rm ADC}}}{V_{\rm ADC}}. \tag{26}$$

The employed $\Delta D_{\rm o}$ is, then, set to

$$\Delta D_{\rm o} = h_{\rm min} \cdot \Delta D_{\rm min} \tag{27}$$

where $h_{\rm min} = \lfloor k_{\rm v}/\Delta D_{\rm min} \rfloor$.

B. Mode Transition to Global MPP Tracking

In the developed OVR algorithm, a transition to global MPP tracking occurs when the dc bus voltage $V_{\rm o}$ falls below its minimum boundary $V_{\rm ref} - \Delta V_{\rm o}$ and the OVR algorithm fails to restore it. The value of $\Delta V_{\rm o}$ represents the absolute maximum allowed tolerance of the dc bus voltage. Failure to restore the dc bus voltage is detected by having a duty ratio equal to $D_{\rm end}$, while having $V_{\rm o}$ below its minimum allowed limit. The global MPP tracking mode is, then, activated. A flowchart representation of both control algorithms is shown in Fig. 6.

IV. Standalone and DC Bus System Applications

In standalone applications that employ energy storage elements as backup, the converter output voltage may also be controlled by the energy storage elements, similar to dc microgrid applications. In such a situation, the proposed global MPP tracking algorithm is still valid without modification. Nonetheless, for standalone applications without energy storage, the converter output voltage is not given. Therefore, the converter output voltage and current have to be measured for accurate tracking. Accordingly, the global MPP tracking algorithm parameters have to be adapted.

Without regulated converter output voltage, the boundaries of the global MPP tracking process are similar to those of the OVR. Therefore, for global MPP tracking, the initial duty ratio $D_{\rm ini}$ obtained in Section III is employed as $D_{\rm min}$. Similarly, the maximum duty ratio $D_{\rm end}$ obtained in Section III is utilized as $D_{\rm max}$. The secondary duty ratio step ΔD_2 is determined from the minimum detectable converter output power change by the ADC in a procedure similar to the one presented in Section II-B4. The primary duty step ΔD_1 is computed to minimize the tracking time as in (14).

The developed OVR algorithm is valid for the standalone applications with the same parameters, as designed in Section III. To sum up, the developed control algorithms are applicable for

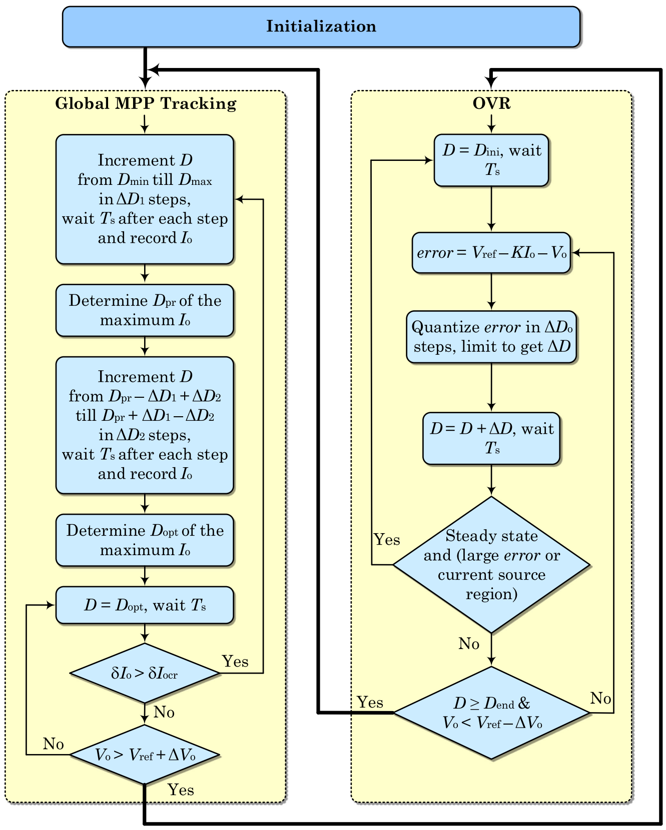

Fig. 6. Flowchart representation of both control algorithms.

standalone applications, following some adaptation of the parameters of the global MPP tracking algorithm.

For the case of PV strings, the proposed global MPP technique is also applicable with some adaptation. This is attributed to the analogy of treating the connection of submodules within the PV module in the same way as considering the connection of modules within the PV string. The main parameters to be adapted are the number of submodules n and the open-circuit voltage V_{oc}. They are to be replaced by the number of modules in the PV string and the open-circuit voltage of the whole string, respectively. In the same context, the MIC parameters are replaced by the parameters of the string converter.

V. Parameter Design

For evaluating the developed control algorithms, the test system and control parameters are designed in this section.

A. *Test System*

A suitable setup is given by a PV module that is integrated into a dc microgrid through an interfacing converter. The PV module has a $V_{\mathrm{oc}} = 44.8$ V, a short-circuit current $I_{\mathrm{sc}} = 5.5$ A, and $n = 3$ submodules. The module is integrated through a boost converter into a low-voltage dc microgrid. The latter consists of a distributed energy resource (DER), a load, and a dc bus. The dc bus voltage is regulated by the DER such that the nominal bus voltage V_{o} is 120 V with an absolute tolerance of 6 V. With input and output ratings suitable for the PV module and dc microgrid, respectively, an interfacing boost converter was designed. The designed specifications are: Output capacitance C_{o} of 2200 μF with an $r_{C_{\mathrm{o}}}$ of 150 mΩ, an inductance L of 0.5 mH with an r_{L} of 85 mΩ, a MOSFET with an ON-resistance r_{DS} of 7.5 mΩ, and a diode with an r_{F} of 61 mΩ.

B. *Control Parameters*

The control parameters of the global MPP tracking followed by the OVR algorithms are calculated. For this purpose, the procedures of Sections II-B and III-A are followed.

The settling time T_{s} is determined from (2) and is set to 50 ms. With its sufficient capabilities, the digital control chip PIC16F877A was chosen for implementing the control algorithms. The chip has $N_{\mathrm{PWM}} = 8$ bits for the PWM module and $N_{\mathrm{ADC}} = 10$ bits for the ADC. Thus, the minimum duty ratio step of the digital control chip $\Delta D_{\min} = 1/2^{N_{\mathrm{PWM}}}$ is about 0.004. From (6), the minimum duty ratio $D_{\min}$ is calculated and adjusted to 0.604. Using (8) and the PV module parameters, a value of 0.908 is assigned to $D_{\max}$. For $V_{\mathrm{ADC}} = 5$ V and a current sensing gain $G_{\mathrm{i}} = 3$, the minimum detectable current change ΔI_{omin} from (10) is equal to 1.63 mA. Thus, using (9), we obtain $k_{\mathrm{i}} = 0.011$. Then, from (12), ΔD_2 is found to be equal to 0.012. From (19), $\Delta D_1 = 0.036$, which is less than the upper limit obtained from (17).

From Section II-C1, δI_{ocr} is defined for resetting the global MPP tracking algorithm. Rather small values of δI_{ocr} may result in a faulty transition to the OVR mode. In contrast, rather large values of δI_{ocr} reduce the sensitivity of the algorithm to irradiance changes. Therefore, δI_{ocr} is set equal to 5 % of the steady-state value of I_{o}. Thus, upon detecting a variation of above 5 % in the steady-state output current, the global MPP tracking algorithm is reset.

For the OVR, D_{ini} is found to be equal to 0.42 using (25). A practical value of 0.95 is assigned to D_{end}. From (26) and for a G_{v} of 1/30, $k_{\mathrm{v}} = 0.007$. Therefore, ΔD_{o} is found to be equal to 0.008.

VI. Prototyping and Validation

The performance of the developed control algorithms is substantiated by physical implementation and testing as follows. At first, the experimental setup is presented. Second, the tests performed for the control algorithms are discussed.

A. *Test Setup*

The setup consists of three main elements. These are the solar array simulator, the dc microgrid, and the interfacing converter, as shown in Fig. 7. In the following, the three elements are described.

1) PV Source: A solar array simulator was adopted in the experimental tests for emulating the performance and characteristics of the PV module. As an alternative, a physical PV module can be utilized. However, the solar array simulator facilitates analyzing several different operating conditions that are independent of local weather conditions and can be reproduced. Therefore, the solar array simulator Agilent E4361A was used.

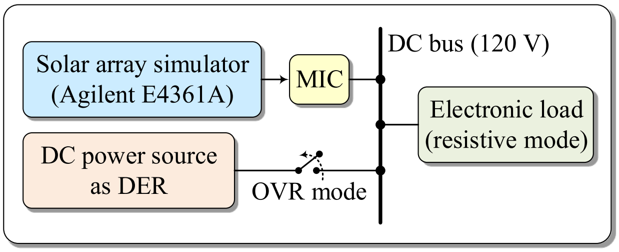

Fig. 7. System configuration of the experimental test setup.

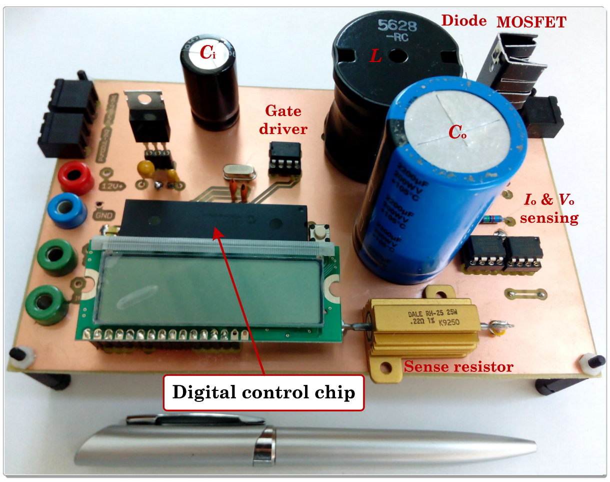

Fig. 8. Employed MIC and its digital control chip.

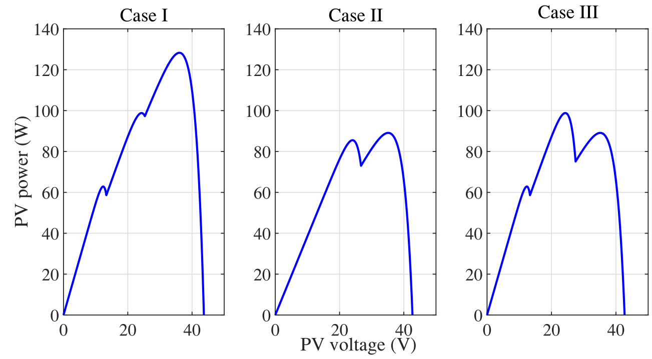

Fig. 9. Power versus voltage characteristics of the three partial shading cases.

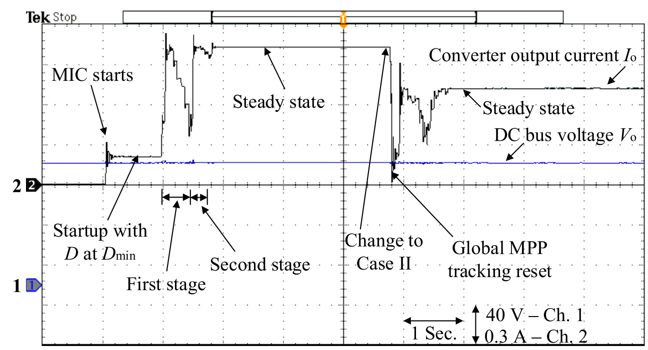

Fig. 10. Global MPP tracking mode waveforms of V_o and I_o under shading patterns of Cases I and II (Ch. 1: 40 V/div, Ch. 2: 0.3 A/div; 1 s/div).

Its table mode with the minimum voltage step of 12 mV was utilized.

2) DC Microgrid and Loads: A dc microgrid for laboratory tests with a dc bus voltage of 120 V was utilized [6], [33]. The MIC is integrated into the dc microgrid as shown in Fig. 1. A DER modeled by a dc power source was employed for regulating the dc bus voltage when the PV module is operated in the global MPP tracking mode. The dc power source was adjusted to emulate the characteristics of a DER. An electronic load operated in its resistive mode with a variable resistance was connected to the dc bus to represent the variable loading of the dc microgrid.

3) Module Integrated Converter: A prototype of the employed MIC was developed for experimental testing, as shown in Fig. 8. The digital control chip PIC16F877A of the MIC was programmed with the developed control algorithms.

B. Experimental Tests

The main performance indicators of the global MPP tracking algorithm are the tracking efficiency, tracking speed, and output oscillations at steady state. These are evaluated under various partial shading patterns, as presented later in this section. For the OVR, the ability to locate the PV operating point at the highest suitable PV voltage for reducing converter power losses and the performance of the dc bus voltage regulation represent the evaluation factors. The performance indicators are investigated in the following through a series of dedicated tests. The mode transition between global MPP tracking and OVR is investigated in the Appendix. Three cases of partial shading are utilized. The PV power versus the PV voltage characteristics of the PV module for these three cases are depicted in Fig. 9. The three patterns feature various numbers of power peaks. The employed test sequences and the corresponding outcomes are as follows.

1) Global MPP Tracking: For evaluating the dynamic and static performances of the developed global MPP tracking algorithm, the tracking efficiency, tracking speed, and output oscillations at steady state are analyzed. For this purpose, the following events are considered while keeping the dc bus voltage continuously regulated by the DER. At first, the shading pattern of Case I with three power peaks is employed in the solar array simulator. This shading pattern is, then, changed to Case II with only two power peaks. This sequence is to test the performance under various shading conditions and power versus voltage characteristics. The corresponding dc bus voltage V_o and the converter output current I_o are measured over time. The results are plotted in Fig. 10. As seen in the plot, the dc bus voltage is kept at 120 V by the DER. It is seen that the MIC is initially inactive with zero output current, and then, the minimum duty ratio is intentionally utilized for a start-up time interval. The measured tracking efficiency, tracking speed, and output oscillations are investigated hereafter.

Tracking efficiency: From Fig. 10 and following the start-up interval, the control algorithm performs the two scanning stages. This is seen through the variations of I_o over time until the peak I_o is reached. Upon detecting a magnitude change of I_o greater than δI_{ocr}, the algorithm is reset, and a new tracking cycle

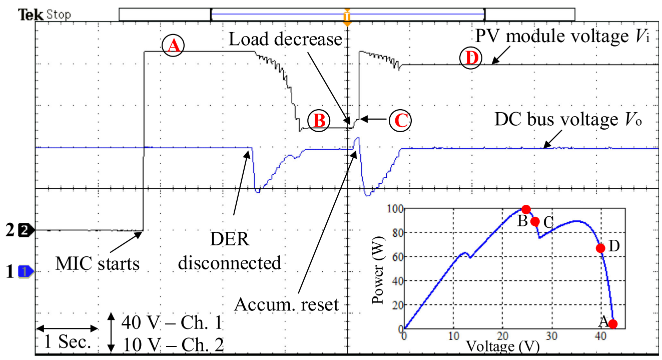

Fig. 11. OVR mode waveforms of V_o and V_i under the shading pattern of Case III and load variation (Ch. 1: 40 V/div, Ch. 2: 10 V/div; 1 s/div).

is performed. This is seen from the variation of I_o when the shading pattern is changed to Case II. For the employed shading patterns of Cases I and II, tracking efficiencies of 99.72 % and 99.82 % were reported by the Agilent E4361A display, respectively. Thus, the results show the high tracking efficiency of the developed global MPP tracking algorithm.

Tracking speed: The time needed to reach the steady state for the two analyzed shading patterns is computed to evaluate the tracking speed. From Fig. 10, scanning intervals of about 0.75 s were measured for the two employed patterns.

Output oscillations: Upon detection of the global peak output current, the control algorithm employs the corresponding duty ratio without any further variations. As a result, the converter output current I_o settles at its maximum without any oscillations. This represents the steady-state operation. Thus, the developed global MPP tracking algorithms fulfills the targets of efficient integration of partially shaded PV modules.

2) OVR: Reducing the power losses in the converter circuit and efficient regulation of the dc bus voltage represent the design targets of the developed OVR algorithm. For the purpose of evaluation, the following test sequence is used over time while employing the shading pattern of Case III in the solar array simulator. At the start, the dc bus voltage is kept regulated by the DER. Second, the DER is deactivated leading to a bus voltage drop, and the MIC is to start regulating the dc bus voltage. Third, the load power is decreased to test the dynamic performance at such a disturbance. In order to assess the bus voltage regulation, the dc bus voltage V_o is measured over time under the aforementioned events. For evaluating the ability to find PV operating points at rather high voltages for a given load, the PV operating points are analyzed. The outcomes are presented in the following.

Effectiveness of regulation: The waveforms of V_i and V_o are depicted in Fig. 11. Initially, the dc bus voltage V_o is at its reference value of 120 V, thanks to the regulation of the DER. Following the disconnection of the DER, the accumulator is reset, and a new scanning cycle is performed. As an outcome, the bus voltage is restored to its reference value. Upon decreasing the load power, the bus voltage exceeds its upper limit. Therefore, the accumulator is reset once again, and a new scanning cycle is executed to restore the dc bus voltage. Following each disturbance, the time taken to restore the bus voltage is about 0.6 s.

TABLE I
COMPARISON OF GLOBAL MPP TRACKING PERFORMANCE

Parameter	Eff. (%)	Speed (s)	Oscillation	Sensors
Technique of [15]	99.60	2.00	Yes	2
Technique of [14]	99.00	3.00	No	2
Technique of [13]	99.70	0.60	No	2
Technique of [18]	99.50	0.38	No	2
Technique of [28]	99.25	3.85	Yes	2
Technique of [19]	98.70	0.10	Yes	4
Technique of [11]	97.00	0.12	Yes	2
Technique of [7]	99.20	0.20	Yes	7
Proposed technique	99.72	0.75	No	1

Reduction of converter power losses: The OVR algorithm is further evaluated by verifying the operation region of the PV module and the corresponding power conversion loss of the MIC. For this purpose, the PV voltage V_i and the operating points on the power versus voltage characteristics are depicted in Fig. 11. Due to the regulation of the dc bus voltage by the DER prior to its disconnection, the dc bus voltage is kept unchanged after activating the MIC. Therefore, the OVR algorithm operates the PV module at its highest voltage represented by point A on the power versus voltage characteristics. In this case, the load power is supplied by the DER. Upon disconnecting the DER, the dc bus voltage is regulated by the MIC, and the PV operation is moved to point B in order to supply a 95-W load. Following the reduction of the load power to around 65 W, the PV operating point moves to C. At that moment, the bus voltage exceeds its upper limit, and thus, the accumulator is reset to D_{ini} to execute a new scanning cycle. Then, the dc bus voltage is restored, and the PV operating point is moved to D. From the PV operating points, it is seen that the PV module is operated at its highest possible voltage.

C. Comparative Performance Analysis

The performance of the developed algorithms is compared with the performance of existing techniques as follows.

1) Global MPP Tracking: The developed global MPP tracking algorithm is evaluated with regard to the tracking efficiency, tracking speed, output oscillations at steady state, and the number of utilized sensors. The results of the comparison are given in Table I. For the techniques presented in [7], [11], [13], [18], and [19], faster global MPP tracking speeds were measured. In terms of the tracking efficiency, output oscillations, and the number of utilized sensors, however, a superior performance is observed.

2) OVR: The performance of the developed OVR algorithm is evaluated by two indicators. These are the bus voltage regulation and the power losses in the converter circuit. In the following, a comparison between the developed algorithm and the existing ones is performed.

With regard to the first indicator, the developed as well as the techniques presented in [20]–[23], [25], and [26] are characterized by a fast and accurate regulation of the dc bus voltage after disturbances. In a detailed comparison, the developed technique enables a highly damped regulation of the dc bus voltage at the expense of a relatively slower settling. Settling times of around 0.48 s were reported in [26], while a settling time of 0.6 s was measured for the developed OVR algorithm. It is to be noted here that the settling time is influenced by the converter elements, as given by (2).

For the second indicator, the PV module is operated at its highest suitable voltage, thanks to the developed OVR algorithm, as seen in Fig. 11. As a result, reduced converter power losses are attained. Through numerous simulations, it was found that the developed OVR algorithm results in around 45 % less converter power losses relative to the power losses obtained with proportional integral controllers [20], [21], [23]. It is to be mentioned that the reduction of the converter power losses within the OVR has not been addressed in the scientific literature. To sum up, the developed OVR algorithm complements the high performance of the global MPP tracking algorithm for efficient integration of the PV modules.

VII. Conclusion

A novel methodology for integrated global MPP tracking and OVR control for partially shaded PV modules was developed, implemented, and its performance compared and tested. With its coarse and fine searching stages, the novel global MPP tracking algorithm achieves experimental tracking efficiencies above 99.72 % within 0.75 s of searching. Meanwhile, the algorithm suppresses any oscillations around the global MPP by the continuous employment of precise duty ratio steps. In addition, the need for periodic scanning of the power versus voltage characteristics for accurate global MPP tracking is avoided, thanks to the novel automated resetting condition, thus facilitating reduced energy losses. The novel global MPP tracking algorithm facilitates reducing the number of employed sensors and the corresponding size, cost, and measurement losses. For the alternate control mode, the developed OVR algorithm allocates the PV operating point in the highest appropriate voltage source region on the PV power versus voltage characteristic. In this manner, it reduces the flowing PV current in the converter circuit to reduce the electric power losses in the circuit elements. As a result, the heat accumulation in the converter circuit is reduced and the corresponding elements' lifetime expectation is enhanced. Thanks to the proposed scanning procedure, the algorithm regulates the dc bus voltage while balancing the power sharing between sources. Simulation and experimental tests as well as a comparative analysis with known existing techniques confirm the convincing overall performance of the control algorithms. This makes the design a compelling solution for the effective integration of PV modules in residential and low-voltage dc microgrids.

Appendix
Mode Transitions

The effectiveness of the developed mode transition conditions is examined through the following simulation. The simulation involves mode transitions by varying the bus voltage and load power over a simulation time interval of 8 s. The global MPP tracking is initially active with the PV module subjected to the shading pattern of Case I. At time 2 s of simulation, the load power is reduced so that the bus voltage exceeds its upper boundary. As a result, a transition from the initial global MPP tracking to the OVR mode is to take place. At that moment, the DER is disconnected from the dc bus, and the PV modules start regulating the dc bus voltage. Then, at time 4 s, a major load power increase takes place. Thus, the load power gets significantly higher than the supplied PV power. As a result of falling dc bus voltage due to the lack of PV power in the OVR mode, the global MPP tracking mode is to be activated automatically.

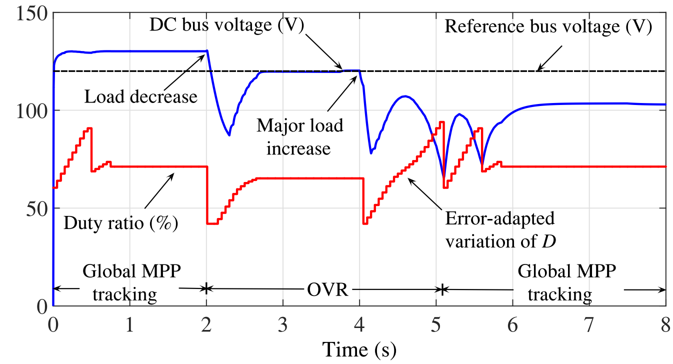

Fig. 12. Time response of V_o and D under mode transitions between global MPP tracking and OVR.

The waveforms of D and V_o corresponding to the simulation time series are depicted in Fig. 12. From the figure and as expected, the transition from global MPP tracking to OVR takes place at 2 s of simulation. This shows the accuracy of the developed mode transition conditions. Moreover, during the time interval from 4 to 5.1 s shown in Fig. 12, the waveform of D shows the proportionality of the variation of D to the dc bus voltage error. It is also to be noted that the unregulated dc bus voltage affects the accuracy of the global MPP tracking when the latter resumes in the time interval starting from 5.1 s. However, the global MPP tracking algorithm has been capable of minimizing the bus voltage error through tracking the maximum available PV power. In conclusion, the performance of both control algorithms with mode transitions fulfill the objectives of smart PV system integration.

Acknowledgment

The authors would like to thank Kerstin Trubel for her support in developing the MIC prototype.

References

[1] K. Strunz, E. Abbasi, and D. N. Huu, "DC microgrid for wind and solar power integration," *IEEE J. Emerg. Sel. Topics Power Electron.*, vol. 2, no. 1, pp. 115–126, Mar. 2014.

[2] G. AlLee and W. Tschudi, "Edison redux: 380 Vdc brings reliability and efficiency to sustainable data centers," *IEEE Power Energy Mag.*, vol. 10, no. 6, pp. 50–59, Nov.–Dec. 2012.

[3] E. Romero-Cadaval, G. Spagnuolo, L. G. Franquelo, C.-Andrés Ramos-Paja, T. Suntio, and W.-Michael Xiao, "Grid-connected photovoltaic generation plants: Components and operation," *IEEE Ind. Electron. Mag.*, vol. 7, no. 3, pp. 6–20, Sep. 2013.

[4] L. Eggenschwiler, M. Adly, P. Favre-Perrod, and K. Strunz, "Closed-loop impedance calculation of grid-tied three-phase inverters/rectifiers in bus signaling strategy-controlled DC microgrids," in *Proc. IEEE 2nd Int. Conf. DC Microgrids*, Jun. 2017, pp. 309–315.

[5] R. C. N. Pilawa-Podgurski and D. J. Perreault, "Submodule integrated distributed maximum power point tracking for solar photovoltaic applications," *IEEE Trans. Power Electron.*, vol. 28, no. 6, pp. 2957–2967, Jun. 2013.

[6] M. Adly and K. Strunz, "Irradiance-adaptive PV module integrated converter for high efficiency and power quality in standalone and DC microgrid applications," *IEEE Trans. Ind. Electron.*, vol. 65, no. 1, pp. 436–446, Jan. 2018.

[7] S. Sajadian and R. Ahmadi, "Distributed maximum power point tracking using model predictive control for photovoltaic energy harvesting architectures based on cascaded power optimizers," *IEEE J. Photovolt.*, vol. 7, no. 3, pp. 849–857, May 2017.

[8] A. M. S. S. Andrade, L. Schuch, and M. L. da Silva Martins, "High step-up PV module integrated converter for PV energy harvest in FREEDM systems," *IEEE Trans. Ind. Appl.*, vol. 53, no. 2, pp. 1138–1148, Mar. 2017.

[9] N. L. Diaz, T. Dragicevic, J. C. Vasquez, and J. M. Guerrero, "Intelligent distributed generation and storage units for DC microgrids—A new concept on cooperative control without communications beyond droop control," *IEEE Trans. Smart Grid*, vol. 5, no. 5, pp. 2476–2485, Sep. 2014.

[10] H. Patel and V. Agarwal, "MATLAB-based modeling to study the effects of partial shading on PV array characteristics," *IEEE Trans. Energy Convers.*, vol. 23, no. 1, pp. 302–310, Mar. 2008.

[11] A. Ramyar, H. Iman-Eini, and S. Farhangi, "Global maximum power point tracking method for photovoltaic arrays under partial shading conditions," *IEEE Trans. Ind. Electron.*, vol. 64, no. 4, pp. 2855–2864, Apr. 2017.

[12] C. Olalla, C. Deline, and D. Maksimovic, "Performance of mismatched PV systems with submodule integrated converters," *IEEE J. Photovolt.*, vol. 4, no. 1, pp. 396–404, Jan. 2014.

[13] J. Ahmed and Z. Salam, "An improved method to predict the position of maximum power point during partial shading for PV arrays," *IEEE Trans. Ind. Inform.*, vol. 11, no. 6, pp. 1378–1387, Dec. 2015.

[14] B. N. Alajmi, K. H. Ahmed, S. J. Finney, and B. W. Williams, "A maximum power point tracking technique for partially shaded photovoltaic systems in microgrids," *IEEE Trans. Ind. Electron.*, vol. 60, no. 4, pp. 1596–1606, Apr. 2013.

[15] H. Patel and V. Agarwal, "Maximum power point tracking scheme for PV systems operating under partially shaded conditions," *IEEE Trans. Ind. Electron.*, vol. 55, no. 4, pp. 1689–1698, Apr. 2008.

[16] T. L. Nguyen and K. S. Low, "A global maximum power point tracking scheme employing DIRECT search algorithm for photovoltaic systems," *IEEE Trans. Ind. Electron.*, vol. 57, no. 10, pp. 3456–3467, Oct. 2010.

[17] Y. Jiang, J. A. Abu Qahouq, and T. A. Haskew, "Adaptive step size with adaptive-perturbation-frequency digital MPPT controller for a single-sensor photovoltaic solar system," *IEEE Trans. Power Electron.*, vol. 28, no. 7, pp. 3195–3205, Jul. 2013.

[18] Y. Wang, Y. Li, and X. Ruan, "High-accuracy and fast-speed MPPT methods for PV string under partially shaded conditions," *IEEE Trans. Ind. Electron.*, vol. 63, no. 1, pp. 235–245, Jan. 2016.

[19] Y. Mahmoud and E. El-Saadany, "A novel MPPT technique based on an image of PV modules," *IEEE Trans. Energy Convers.*, vol. 32, no. 1, pp. 213–221, Mar. 2017.

[20] L. Qin, S. Xie, M. Hu, and C. Yang, "Stable operating area of photovoltaic cells feeding DC–DC converter in output voltage regulation mode," *IET Renewable Power Gener.*, vol. 9, no. 8, pp. 970–981, Nov. 2015.

[21] W. Xiao, W. G. Dunford, P. R. Palmer, and A. Capel, "Regulation of photovoltaic voltage," *IEEE Trans. Ind. Electron.*, vol. 54, no. 3, pp. 1365–1374, Jun. 2007.

[22] J. A. Gow and C. D. Manning, "Controller arrangement for boost converter systems sourced from solar photovoltaic arrays or other maximum power sources," *IEE Proc.—Electric Power Appl.*, vol. 147, no. 1, pp. 15–20, Jan. 2000.

[23] M. G. Villalva, T. G. D. Siqueira, and E. Ruppert, "Voltage regulation of photovoltaic arrays: Small-signal analysis and control design," *IET Power Electron.*, vol. 3, no. 6, pp. 869–880, Nov. 2010.

[24] S. Augustine, N. Lakshminarasamma, and M. K. Mishra, "Control of photovoltaic-based low-voltage DC microgrid system for power sharing with modified droop algorithm," *IET Power Electron.*, vol. 9, no. 6, pp. 1132–1143, May 2016.

[25] M. Sitbon, S. Schacham, and A. Kuperman, "Disturbance observer-based voltage regulation of current-mode-boost-converter-interfaced photovoltaic generator," *IEEE Trans. Ind. Electron.*, vol. 62, no. 9, pp. 5776–5785, Sep. 2015.

[26] G. C. Konstantopoulos and A. T. Alexandridis, "Non-linear voltage regulator design for DC/DC boost converters used in photovoltaic applications: Analysis and experimental results," *IET Renewable Power Gener.*, vol. 7, no. 3, pp. 296–308, May 2013.

[27] M. Andresen and M. Liserre, "Impact of active thermal management on power electronics design," *Microelectron. Rel.*, vol. 54, no. 9–10, pp. 1935–1939, Aug. 2014.

[28] C. Manickam, G. R. Raman, G. P. Raman, S. I. Ganesan, and C. Nagamani, "A hybrid algorithm for tracking of GMPP based on P&O and PSO with reduced power oscillation in string inverters," *IEEE Trans. Ind. Electron.*, vol. 63, no. 10, pp. 6097–6106, Oct. 2016.

[29] A. Sangwongwanich, Y. Yang, D. Sera, H. Soltani, and F. Blaabjerg, "Analysis and modeling of interharmonics from grid-connected photovoltaic systems," *IEEE Trans. Power Electron.*, vol. 33, no. 10, pp. 8353–8364, Oct. 2018.

[30] M. K. Kazimierczuk, *Pulse-Width Modulated DC–DC Power Converters*. West Sussex, U.K.: Wiley, 2008.

[31] K. Ogata, *Modern Control Engineering*. New Jersey, NJ, USA: Pearson, 2009.

[32] M. Boztepe, F. Guinjoan, G. Velasco-Quesada, S. Silvestre, A. Chouder, and E. Karatepe, "Global MPPT scheme for photovoltaic string inverters based on restricted voltage window search algorithm," *IEEE Trans. Ind. Electron.*, vol. 61, no. 7, pp. 3302–3312, Jul. 2014.

[33] C. Wiezorek *et al.*, "Multi-location virtual smart grid laboratory with testbed for analysis of secure communication and remote co-simulation: Concept and application to integration of Berlin, Stockholm, Helsinki," *IET Gener. Transmiss. Distrib.*, vol. 11, no. 12, pp. 3134–3143, Sep. 2017.

Moustafa Adly (S'14) received the B.Sc. degree in electronics and electrical communications from Cairo University, Cairo, Egypt, in 2004, and the M.Sc. degree in electronics and electrical energy systems from the German University in Cairo, New Cairo City, Egypt, in 2011. In 2018, he received the Ph.D. degree from the Technische Universität Berlin, Berlin, Germany.

He was with Cairo University and the German University in Cairo as a Researcher and Lecturer Assistant. He is a Researcher with teaching duties with the Technische Universität Berlin. He is currently actively contributing to the electric vehicles industry in Germany. His research interests include PVs, power electronics, digital and embedded control systems, and dc power systems.

Dr. Adly is a Reviewer for several international journals including the IEEE TRANSACTIONS.

Kai Strunz received the Dipl.-Ing. and Dr.-Ing. (summa cum laude) degrees from Saarland University, Saarbrücken, Germany, in 1996 and 2001, respectively. From 1995 to 1997, he pursued research at Brunel University, London, U.K.

From 1997 to 2002, he was with the Division Recherche et Développement of Electricité de France in the Paris area. From 2002 to 2007, he was an Assistant Professor of electrical engineering with the University of Washington, Seattle, WA, USA. Since September 2007, he has been a Professor for sustainable electric networks and sources of energy with Technische Universität Berlin, Germany. He is a Guest Professor with the Chinese Academy of Sciences, Beijing, China.

Dr. Strunz was the recipient of the IEEE PES Prize Paper Award in 2015 and the IEEE JOURNAL OF EMERGING AND SELECTED TOPICS IN POWER ELECTRONICS First Prize Paper Award in 2015. He was the Chairman of the IEEE PES Innovative Smart Grid Technologies Conference held at Technische Universität Berlin in 2012. He is the Chairman of the IEEE Power and Energy Society (PES) Subcommittee on Distributed Energy Resources. On behalf of the Intergovernmental Panel on Climate Change, he was a Review Editor for the Special Report on Renewable Energy Sources and Climate Change Mitigation.